

Developing a mouse model of acute encephalopathy using low-dose lipopolysaccharide injection and hyperthermia treatment

Hirofumi Kurata^{1,2,3} , Kengo Saito¹, Fumiaki Kawashima¹, Takuya Ikenari¹, Masayoshi Oguri⁴, Yoshiaki Saito², Yoshihiro Maegaki² and Tetsuji Mori¹

¹Department of Biological Regulation, School of Health Science, Faculty of Medicine, Tottori University, Yonago 683-8503, Japan;

²Division of Child Neurology, Department of Brain and Neurosciences, Tottori University, Yonago 683-8504, Japan; ³Department of Pediatrics, National Hospital Organization, Kumamoto Saishunso National Hospital, Koshi, 861-1196, Japan; ⁴Department of Pathobiological Science and Technology, School of Health Science, Faculty of Medicine, Tottori University, Yonago 683-8503, Japan
Corresponding authors: Hirofumi Kurata. Email: kurata0708@hotmail.com; Tetsuji Mori. Email: mori-te@tottori-u.ac.jp

Impact statement

Acute encephalopathy (AE), mainly reported in East Asia, is classified into four categories based on clinical and neuropathological findings. Among them, AE caused by cytokine storm is known as the severest clinical entity that causes cerebral edema with poor prognosis. Because suitable and convenient model animal of AE had not been developed, the treatment of patients with AE is not established. In the present study, we established a simple and convenient protocol to mimic AE due to cytokine storm. Our model animal should be useful to elucidate the pathogenesis of AE.

Abstract

Acute encephalopathy (AE) is mainly reported in East Asia and, in most cases, results from pediatric viral infections, leading to fever, seizure, and loss of consciousness. Cerebral edema is the most important pathological symptom of AE. At present, AE is classified into four categories based on clinical and pathophysiological features, and cytokine storm-induced AE is the severest among them. The pathogenesis of AE is currently unclear; this can be attributed to the lack of a simple and convenient animal model for research. Here, we hypothesized that the induction of systemic inflammation using lipopolysaccharide (LPS) injection followed by hyperthermia (HT) treatment can be used to develop an animal model of cytokine storm-induced AE. Postnatal eight-day-old mouse pups were intraperitoneally injected with low-dose LPS (50 or 100 µg/kg) followed by HT treatment (41.5°C, 30 min). Histological analysis of their brains was subsequently performed.

Fluorescein isothiocyanate assay combined with immunohistochemistry was used to elucidate blood–brain barrier (BBB) disruption. LPS (100 µg/kg) injection followed by HT treatment increased BBB permeability in the cerebral cortex and induced microglial activation. Astrocytic clasmatodendrosis was also evident. The brains of some pups exhibited small ischemic lesions, particularly in the cerebral cortex. Our results indicate that a low-dose LPS injection followed by HT treatment can produce symptoms of cytokine storm-induced AE, which is observed in diseases, such as acute necrotizing encephalopathy and hemorrhagic shock and encephalopathy syndrome. Thus, this mouse model can help to elucidate the pathogenetic mechanisms underlying AE.

Keywords: Hyperthermia, lipopolysaccharide, seizure, blood–brain barrier, vasogenic edema, acute encephalopathy

Experimental Biology and Medicine 2019; 244: 743–751. DOI: 10.1177/1535370219846497

Introduction

Febrile acute encephalopathy (AE), a severe condition characterized by cerebral edema, is mainly reported in East Asia and results from pediatric viral infections caused by microbes, such as influenza virus, human herpesvirus 6, and rotavirus. It is notable that although bacterial pathogens, such as *Escherichia coli* and *Salmonella enteritidis*, can cause AE in some cases, they have rarely been detected as pathogens causing AE.¹ Children affected by AE due to

infectious diseases exhibit fever, seizure, and loss of consciousness, often leading to death. Currently, AE is classified into the following four categories based on clinical and neuropathological findings: metabolic error-induced AE, cytokine storm (hypercytokinemia)-induced AE, excitotoxicity-induced AE, and AE with unknown pathogenesis.² Of these, cytokine storm-induced AE manifests as increased proinflammatory cytokine production and has the worst severity and prognosis (associated mortality is

approximately 30–50%).^{1–5} Patients who survive cytokine storm-induced AE suffer from severe neurological sequelae, such as mental retardation and motor paralysis.^{1,4} Moreover, this category includes acute necrotizing encephalopathy (ANE)⁶ and hemorrhagic shock and encephalopathy syndrome (HSES),⁷ which primarily present as blood–brain barrier (BBB) disruption leading to cerebral vasogenic edema.^{2,8}

Neuropathological findings of patients with ANE include multifocal, symmetric brain lesions affecting the bilateral thalami, putamina, brain stem tegmentum, and cerebral and cerebellar white matter; necropsy findings include cerebral edema, brainstem hemorrhage, and neuronal necrosis, suggesting BBB disruption.^{2,6,8,9} In addition, neuropathological examination following necropsy in patients with HSES revealed brain edema and neuronal necrosis as well as petechial hemorrhage surrounding small vessels and multiple ischemic injuries, including hemorrhagic infarction.^{2,10} In severe cases, diffuse necrotic changes and brain liquefaction, a condition termed as “respirator brain,” are evident.^{8,11–17} In addition, both ANE and HSES lead to the failure of multiple organs associated with disseminated intravascular coagulation, including the liver and kidney.²

Although it has been hypothesized that upregulation of proinflammatory cytokines is the key factor of AE,¹⁸ its pathogenesis and neurophysiology remain largely unclear. The inability to elucidate its pathophysiology, and subsequently, to develop therapeutic methods can be attributed to the lack of a simple and convenient animal model for research. A mouse model of influenza-associated encephalopathy (IAE) has been developed from pulmonary infection with influenza A virus and lipopolysaccharide (LPS, 0.5 mg/kg) injection; however, dedicated biosafety facilities for handling the pathogenic virus are essential for using this model.¹⁹ Thus, an improved and more convenient animal model is necessary.

The onset of ANE and HSES occurs during the early febrile period of a viral infection. Accumulating evidence indicates that low-dose (0.05–0.2 mg/kg)^{20–22} and high-dose (1 mg/kg)²³ LPS injections can induce systemic inflammation with modest and transient upregulation of proinflammatory cytokines in neonatal rodents. Along with upregulation of proinflammatory cytokines at acute phase in neonatal rodents, a low-dose LPS injection induces microglial activation,^{22,24} but not astrocyte responses,²⁵ whereas a high-dose LPS injection induces transient BBB disruption.²³ However, another study has reported conflicting effects of low-dose LPS (0.3 mg/kg) injections in neonatal rat pups, wherein neither BBB disruption nor microglial activation was observed.²⁶ Even high-dose LPS (1 mg/kg) injections do not result in any permanent neuronal losses in the hippocampus, a brain region vulnerable to various insults.²⁷ Alternatively, an experimental neonatal rodent model of prolonged febrile seizures requiring 30 min of hot-air treatment to induce hyperthermia (HT) is widely used²⁸; in this model, HT treatment induces generalized tonic-clonic seizure (GTCS).²² Moreover, HT treatment induces transient proinflammatory cytokine level upregulation,^{22,29–31} but does not result in obvious

neuronal losses in the hippocampus.³² These data indicate that neither low-dose LPS injections nor HT treatment alone can induce AE symptoms.

We hypothesized that the induction of systemic inflammation using LPS injection followed by HT treatment can be used to develop an animal model of cytokine storm-induced AE. Studies performed in rodent pups administered with low-dose LPS injections followed by HT treatment have demonstrated increased neuronal excitability, and those performed in pups receiving low-dose LPS injections have demonstrated susceptibility to HT-induced seizures.^{22,33} Although a low-dose LPS injection followed by HT treatment upregulates seizure-induced proinflammatory cytokine production and microglial activation, detailed pathologic analyses of the brains of these animals are warranted.²²

Here, we tested our hypothesis that a low-dose LPS injection followed by HT treatment leads to BBB disruption and induces cerebral vasogenic edema in mouse pups. In addition, the cerebral cortices of the treated mouse pups were analyzed for histopathological changes similar to those observed in the cerebral cortices of patients with AE.

Materials and methods

Animals

Pregnant ICR mice were supplied by Japan SLC (Shizuoka, Japan). Postnatal day (P) eight mouse pups of both sexes were used. Pups and their lactating dams were housed in rack-mounted cages and maintained under a 12 h light/dark cycle. All experiments were conducted in accordance with the Guidelines for Animal Experimentation, Faculty of Medicine, Tottori University under the International Guiding Principles for Biomedical Research Involving Animals.

LPS administration

LPS (*E. coli*, serotype O127:B8; Sigma, St Louis, MO, USA) was dissolved in sterile pyrogen-free phosphate buffered saline (PBS, pH 7.0) at concentrations of 5 or 10 µg/mL. LPS was intraperitoneally (ip) injected at a dose of 50 or 100 µg/kg 2 h before HT treatment (Figure 1(a)). For control pups, the same volume of sterile pyrogen-free PBS was injected.

Based on what was administered to the pups, they were categorized into five groups: PBS (control, $n=8$), LPS 100 µg/kg only (LPS100, $n=8$), HT only (HT, $n=8$), LPS 50 µg/kg + HT (LPS50 + HT, $n=19$), and LPS 100 µg/kg + HT (LPS100 + HT, $n=8$) (Figure 1(a)). From each group, three pups were randomly selected and used for FITC leakage analysis (see below).

HT treatment and seizure induction

Hyperthermic seizures were induced using a heat lamp, as previously reported.²² The rectal temperature in pups was continuously monitored using a rectal probe (RET-4; Physitemp Instruments, Clifton, NJ, USA) connected to a multipurpose thermometer (BAT-10; Physitemp Instruments). P8 mice were placed in a transparent

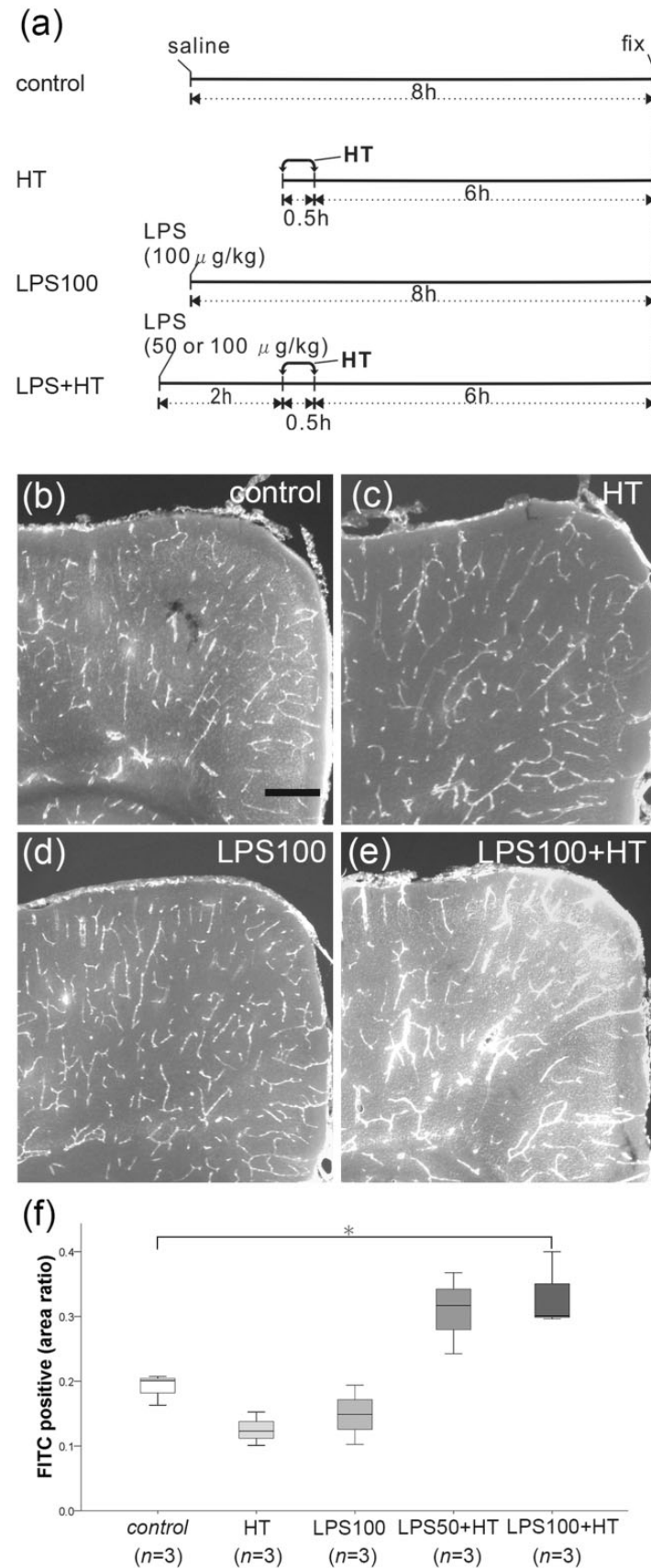


Figure 1. BBB disruption in the LPS100 + HT group. (a) Schematic representation of the treatment protocol. Epi-fluorescence microscopy images of FITC labeling in the cingulate cortex indicating the control (b), HT (c), LPS100 (d), and LPS100 + HT (e) groups. (f) The proportion of the FITC-positive cortical area is compared among the experimental groups. The proportion of the FITC-positive cortical area significantly increased in the LPS100 + HT group compared with that in the control group. $n = 3$ in each group, *: $p < 0.05$, one-way analysis of variance followed by Tukey's multiple comparison test. Scale bar: 300 μ m. FITC: fluorescein isothiocyanate; HT: hyperthermia; LPS: lipopolysaccharide.

container and were heated using the heat lamp. The rectal temperature was increased by 0.5°C every 2 min and was maintained at >39°C for 30 min. Heating was discontinued when a convulsion was noted or when the rectal temperature exceeded 41.5°C. HT treatment was resumed when the rectal temperature decreased to <40°C and seizure interruption was confirmed. Behavioral seizures in pups were limited to GTCS and excluded any other movements that could be recognized as part of a partial seizure. After 30 min of HT treatment, the pups were placed in a cool container containing water-soaked paper towels until their rectal temperatures returned to normal (33–35°C) and then placed back in their cages. At 6 h after HT treatment, survived pups were perfused with FITC for histological analysis, as described further in the text below.

FITC perfusion followed by alkaline paraformaldehyde fixation

A new technique developed by Miyata and Morita³⁴ was employed for visualizing cerebral vasculature and BBB disruption in brain tissue sections in combination with histological analysis via fluorescent immunostaining. Briefly, the pups were euthanized using pentobarbital (50 mg/kg, ip) and intracardially perfused with PBS (pH 7.0) for 2 min, followed by perfusion of 0.1 mg/mL fluorescein isothiocyanate isomer-I (FITC, Dojindo, Tokyo, Japan) in PBS (pH 7.0) for 7 min. They were then perfused with PBS (pH 7.0) for 3 min to wash out any remainder intravascular FITC and fixed by intracardiac perfusion with 4% paraformaldehyde (PFA) in 0.1 M phosphate buffer (PB; pH 8.0) for 7 min. The treated brains were extracted and postfixed with the same fixative overnight. All the brains were then cryoprotected with 20% sucrose in PBS. Other organs (liver and kidney) were also extracted and embedded in paraffin.

Histological procedures

The brains were embedded in Super Cryo Mount (Muto Pure Chemicals, Tokyo, Japan) and snap frozen on dry ice. Free-floating, 30-μm-thick coronal sections were transversely cut using a cryostat (model OT; Bright Instruments, Bedfordshire, UK). The sections were then incubated with the following primary antibodies: mouse anti-GFAP (glial fibrillary acidic protein, 1:400; Sigma), rabbit anti-Iba1 (1:1000; Wako Chemicals, Tokyo, Japan), mouse anti-NeuN (1:200; Millipore, Temecula, CA, USA), rabbit anti-activated Caspase-3 (1:400; Promega, Madison, WI, USA), or rabbit anti-CD31 antibody (1:100; Abcam, Cambridge, UK). Primary antibodies were detected using species-specific secondary donkey antibodies conjugated to Alexa Fluor 555 (1:800, Invitrogen, Carlsbad, CA, USA), Alexa Fluor 647 (1:800; Thermo Fisher Scientific, Pittsburgh, PA, USA), or Cy3 (1:200; Jackson ImmunoResearch, West Grove, PA, USA). For visualizing nuclei, the immunostained sections were mounted onto glass slides, with mounting media containing 0.2% n-propyl gallate, 50% glycerol, and 5 μg/mL Hoechst 33258 in PBS, and covered using coverslips. The paraffin-embedded livers and kidneys were cut into 4- and 3-μm-thick sections, respectively,

and were processed for hematoxylin and eosin (H&E) staining according to the standard protocol.

Image acquisition and analysis

Single optical confocal microscopy images were acquired using the LSM 780 microscope with a 40× objective lens (Carl Zeiss, Oberkochen, Germany) and were stacked using the ZEN software (Carl Zeiss). The vasculature of the subventricular zone is physiologically permeable owing to the relative lack of blood vessel coverage by astrocytic endfeet and pericyte.^{35,36} Moreover, circumventricular organs contain permeable fenestrated capillaries and lack the BBB.³⁷ Hence, we quantified the BBB permeability in the cerebral cortex at the level of the anterior commissure. For this, brain images were acquired using the BIOREVO BZ-9000 epi-fluorescence microscope (Keyence, Osaka, Japan) with a 10× objective lens. Sites demonstrating BBB disruption were identified using FITC staining, and the corresponding sections were analyzed using the ImageJ program (<https://imagej.nih.gov/ij/>). Because FITC leakage was never observed in the corpus callosum, the image brightness was normalized to that of the corpus callosum. The FITC-stained images were converted to black and white binary images, and the stained areas were automatically quantified using the particle analysis function of the ImageJ program. The entire cortical area was also assessed using the ImageJ program to calculate the proportion of the FITC-positive cortical area.

Statistical analysis

One-way analysis of variance followed by Tukey's multiple comparison test was conducted to compare the differences in the proportions of the FITC-positive cortical areas among the experimental groups. Three mice randomly selected from each group were analyzed. The statistical significance was set at $p < 0.05$. All statistical analyses were performed using the SPSS Statistics 24.0 software (IBM, Tokyo, Japan).

Results

LPS exacerbates HT insult

All pups in the HT groups (HT, LPS50 + HT, and LPS100 + HT) exhibited GTCS, whereas none in the control and LPS100 groups exhibited seizures. Some complex partial seizures with chewing automatism, limb clonus, and limb stiffening sometimes progressed to GTCS. Varying onset times of behavioral arrest, ptialism, and vomiting were noted in some cases. The mortality rates in the LPS100 + HT and LPS50 + HT groups (58.8 and 32.1%, respectively) were high, whereas that in the HT group was low (12.5%). Moreover, all mouse pups in the LPS100 and control groups survived.

BBB disruption in the LPS100 + HT group

Of all the treatment groups, only the LPS100 + HT group demonstrated a significantly higher proportion of the FITC-positive cortical area than the control group (Figure 1(b) to (f)). Although the LPS50 + HT group had a moderate

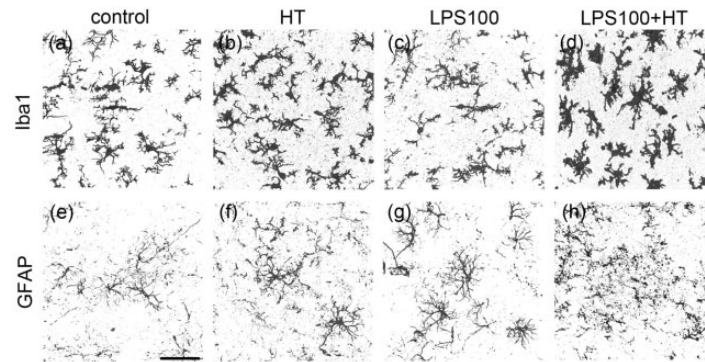


Figure 2. Morphologies of microglia and astrocytes in each experimental group. Stacked confocal microscopy images of Iba1(+) microglia (a to d) and GFAP(+) astrocytes (e to h) in each group: control (a, e); HT (b, f); LPS100 (c, g); LPS100 + HT (d, h) groups. Iba1(+) microglia exhibit an amoeboid form in the LPS100 + HT group (d). GFAP(+) processes in the LPS100 + HT group are fragmented (h). No or moderate morphological changes are detected in the other groups (a to c and e to g). Scale bar: 50 μ m. GFAP: glial fibrillary acidic protein.

mortality rate, the proportion of the FITC-positive cortical area did not significantly increase compared with that in the control, HT, and LPS100 groups (Figure 1(f)). In contrast, LPS100 + HT treatment resulted in the exacerbation of BBB disruption, which was confirmed by an increased proportion of the FITC-positive cortical area (Figure 1(f)). The FITC signal was detected both in the vasculature and brain parenchyma (Figure 1(e)). Light microscopic observation of the H&E-stained liver and kidney specimens revealed no notable changes between the control and LPS100 + HT groups (data not shown).

Microglial activation and astrocytic clasmotodendrosis in the LPS100 + HT group

Microglial and astrocytic responses to treatment were assessed using anti-Iba1 and anti-GFAP antibodies, respectively. In the LPS100 + HT group, almost all the microglia were morphologically activated when compared with other groups (Figure 2(a) to (d)); the microglia exhibited an amoeboid shape with an enlarged cell-body size and more elaborate processes (Figure 2(d)). There was no obvious localization of the activated microglia in the LPS100 + HT group (data not shown).

The astrocytes also exhibited a reactive state in the LPS100 + HT group, with prominent processes and enlarged cell bodies (Figure 2(e) to (h), Supplemental Fig. 1). Notably, some astrocytes exhibited a loss in processes, leading to fragmentation, as indicated by the diffused GFAP signals; this irreversible morphological change is characteristic to astrocytic clasmotodendrosis³⁸ (Figure 2(h)). The reactive state and severity of clasmotodendrosis in reactive astrocytes varied between each pup in the LPS100 + HT group (Figures 2(h) and 3(e) and Supplemental Fig. 1(b)). In addition, there was no obvious localization of reactive astrocytes with clasmotodendrosis in the cortical gray matter. Double immunostaining for anti-Iba1 and anti-GFAP antibodies revealed overlapping signals, suggesting the phagocytosis of astrocytes by microglia (Figure 3(h), arrow). Phagocytic images could be acquired in any region of the cortical gray matter where clasmotodendrosis of astrocytes was detected. The nuclear

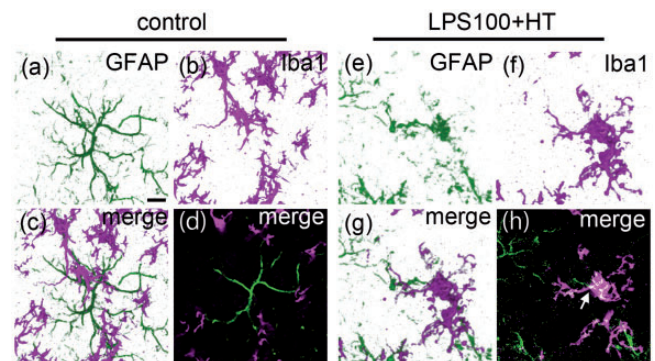


Figure 3. Presumptive phagocytosis by microglia in the LPS100 + HT group. Stacked (a to c and e to g) and single optical (d and h) confocal microscopy images in the cerebral cortex of the control (a to d) and LPS100 + HT (e to h) groups. The phagocytosis of a swollen and fragmented GFAP(+) astrocyte (green) by Iba1(+) activated microglia (magenta) is evident in the LPS100 + HT group (e to h). The single optical section reveals the co-localization of GFAP and Iba1 signals (white, arrow) (h). These overlaps between the GFAP and Iba1 signals are not detected in the control group (d). Scale bar: 10 μ m.

morphology of the cerebrocortical neurons indicated no neuronal death (data not shown).

Small cortical ischemic sites in some pups in the LPS100 + HT group

Interestingly, two of the eight pups in the LPS100 + HT group exhibited several small spots with an extremely faint or nonexistent FITC signal in the cerebral cortex (Figure 4(a), white arrowheads). H&E staining revealed that these spots represented dying neurons with vacuolation, damaged neuropil, pyknotic nuclei, and eosinophilic cell bodies (Figure 4(b) and (c), white arrowheads, black arrowheads, and arrows). Moreover, NeuN immunoreactivity, a marker that is used for identifying mature neurons and that demonstrates neurodegeneration, decreased in these spots (Supplemental Fig. 2). Activated Iba1 immunopositive (+) microglial invasion was noted in these spots (Supplemental Fig. 3). To analyze these degenerating neurons, immunostaining with antiactivated Caspase 3 antibody (Cas3), a marker of apoptosis, was performed. The results indicated that the number of Cas3(+) cells did not

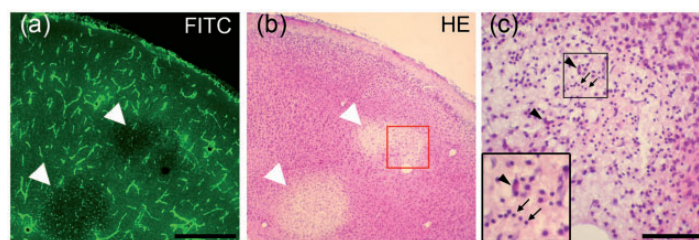


Figure 4. Spots devoid of FITC signals in the LPS100 + HT group. Epi-fluorescence microscopy image of FITC in the cerebral cortex (a). The same section stained using H&E is shown in (b). The FITC-devoid spots are indicated by white arrowheads. The boxed area in (b) contains dying neurons with eosinophilic cell bodies (black arrowheads) and pyknotic nuclei (arrows) (c). Scale bar: 500 μ m (a) and 100 μ m (c). H&E: hematoxylin and eosin.

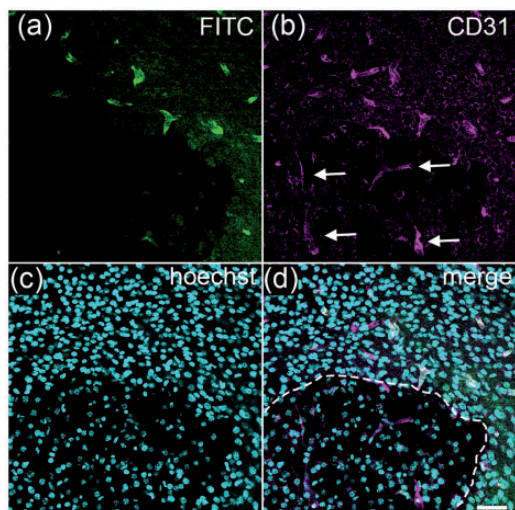


Figure 5. Focal cerebral ischemia in the LPS100 + HT group. An FITC-devoid spot (a) containing CD31(+) minute vessels (b, arrows). Hoechst33258 (c) and merged images (d) distinctly show the edge of the spot (dashed line, d). Pyknotic nuclei visualized with Hoechst33258 staining are visible in the spot. Single optical confocal microscopy images are shown. Scale bar: 50 μ m.

significantly increase in these spots (data not shown). Anti-CD31 antibody staining, a marker of vascular endothelial cells, identified minute blood vessels and endothelial cells despite the lack of FITC signals in these areas (Figure 5, arrows).

Discussion

In the present study, a model of cytokine storm-induced AE generated by treating pups with LPS100 + HT demonstrated relatively mild BBB disruption, microglial activation, and clasmotodendrosis of astrocytes. These histopathological changes are crucial in the assessment of ANE and HSES.

BBB disruption is recognized on non-invasive brain imaging results in patients with AE, which is extremely important for clinically diagnosing AE.^{8,9} Although histopathological data are essential to elucidate the pathogenesis of AE, they are limited owing to ethical concerns and the low incidence of AE. For experimental animals, Evans Blue (molecular weight, 960.81) is commonly used for evaluating BBB disruption^{19,39,40} However, Evans Blue tightly and rapidly binds to serum albumin (molecular weight, 69,000),^{40,41} implying that it can be used only in cases of

severe BBB disruption, such as in cases of brain trauma and the filamentous occlusion of the middle cerebral artery.⁴²

In contrast, FITC (molecular weight, 389.38) is a low-molecular weight tracer that is fixable on tissue sections using PFA at an alkaline pH.³⁴ Thus, owing to its higher sensitivity than Evans Blue, we used FITC to visualize and identify the vasculature and BBB disruption in tissue sections.³⁴ Evans Blue leakage could not be evidently detected using light and fluorescence microscopy in the preliminary experiments in the LPS100 + HT group (data not shown). However, FITC leakage was evident in the LPS100 + HT group. These findings suggest that the BBB disruption in the LPS100 + HT group was mild or at an early stage and that only small molecules passed through the walls of the blood vessels.

Our results showed that the combination of systemic inflammation and HT was the key factor for inducing an AE-like state in the model. Regarding the degree of inflammation, high-dose LPS (1–3 mg/kg) injections without HT are known to induce BBB disruption in rodent pups.^{43,44} Wang *et al.*²⁶ have reported that a single ip injection of low-dose LPS (300 μ g/kg) without HT in P7 rats did not influence tight junctions of cerebral endothelial cells nor induce BBB disruption or microglial activation. Although certain conflicting observations were noted,²³ our results supported the data reported by Wang *et al.* that no significant difference was noted in the proportion of the FITC-positive area in the cerebral cortex between the control and LPS100 groups. For the application of HT, prolonged HT itself does not elicit serious, permanent effects on the neonatal rodent brains.^{22,32} Our results corroborate with the results of these studies in that no significant differences were noted regarding FITC leakage in the HT and control group.

In contrast, low-dose LPS injections exacerbate subsequent insults, such as hypoxia and HT.^{22,33,45} Indeed, the present study demonstrated that the pups in the LPS100 + HT group had significantly greater FITC leakage and the highest mortality among all groups. Notably, 50 μ g/kg LPS was inadequate to exacerbate the effects of subsequent HT, probably owing to the LPS dose-dependent upregulation of proinflammatory cytokines.⁴⁶ It has been clearly demonstrated that prolonged HT treatment itself induces proinflammatory cytokine upregulation.^{22,29–31} Considering these results, only a sufficient elevation in the proinflammatory cytokine level followed by HT treatment can replicate the histopathological changes in a

mouse model of cytokine storm-induced AE. The procedure is simple and does not require special facilities; hence, it can be applicable to other species as well.

Cytokine storm-induced AE results in high mortality (30–50%) in humans. In the present study, the LPS100 + HT group exhibited the highest mortality (58.8%). Furthermore, LPS100 + HT treatment induced significant BBB disruption and microglial activation with an amoeboid shape and elaborate processes. These neuropathological findings are frequently detected in patients with AE.^{2,6,8,9} A notable finding of our study is that the LPS100 + HT group exhibited astrocytic clasmotodendrosis and putative phagocytosis of degenerating astrocytes by activated microglia. Astrocytic clasmotodendrosis is characterized by swollen cell cytoplasm and vacuolated cell bodies with beaded and fragmented processes and is associated with various degenerative disorders in human patients, including Alzheimer's disease, poststroke dementia, mixed dementia, and Ataxia telangiectasia^{47–52} as well as in experimental conditions.^{53,54} In fact, the postmortem immunohistochemical analysis of the brains of all patients with ANE and HSES has confirmed the presence of clasmotodendritic astrocytes.^{9,52,55,56} The mechanism of cell death in astrocytes is different in each disease, for example necrosis, apoptosis, and autophagy. Recently, it was suggested that clasmotodendrosis of astrocytes in IAE patients represents the acute phase of necrosis.⁵² At present, it is unclear whether necrotic death of astrocytes is a common mechanism of cell death in all types of AE. Further studies are required to investigate this.

Another notable finding of the present study is that 25% (two of eight) of the LPS100 + HT pups had presumptive ischemic spots in the cerebral cortex that were almost devoid of FITC leakage. These spots were found to have CD31(+) endothelial cells and Cas3-immunonegative necrotizing neurons, indicating that these resulted from focal ischemia. Both ANE and HSES show similar neuropathological findings, such as neuronal necrosis resulting from vasogenic edema, owing to BBB disruption and multiple organ failure associated with disseminated intravascular coagulation.² However, because ischemia in HSES is widespread,¹⁰ the LPS100 + HT pups with focal ischemia could serve as a suitable model of HSES.

Some inconsistent pathological data were noted between the LPS100 + HT pups and patients with AE. First, neuronal necrosis, an important symptom of AE,^{2,6,8,9} was limited to the FITC-devoid spots in the brain specimens of the LPS100 + HT pups. Second, BBB disruption was relatively mild, which was inferred from the passage of relatively small molecules through the walls of the blood vessels, whereas hemorrhage and plasma leakage is common in most patients with HSES and ANE.^{2,6,8} Third, although the number of Cas3(+) cells considerably increases in some human autopsy cases with IAE,^{2,9} the number of Cas3(+) (apoptotic) cells did not significantly increase. Fourth, although various non-specific pathological changes (e.g. systemic petechial hemorrhage, pneumonia, renal infarction, and fatty changes of the liver) were noted in patients with ANE and HSES,^{6,12,14,17} no obvious pathological changes were noted in the liver and kidney of the pups

in the present study. These differences could be attributed to the timing of tissue sampling; autopsy samples were obtained much later than those obtained from our mouse model after the onset of AE symptoms, such as fever and seizures. Further studies are warranted to confirm this effect of the timing of tissue sampling.

The neuropathological changes observed in our mouse model were primarily attributed to proinflammatory cytokines induced by low-dose LPS injection and HT. Meanwhile, certain genetic factors can precipitate the emergence of AE in humans. For example, AE is a regional syndrome occurring mainly in East Asia, which suggests that the genetic background could be involved in the pathogenesis. In addition, some gene variations in humans affect their susceptibility to AE. Mutations in the sodium voltage-gated channel alpha subunit 2 and Ran-binding protein 2 cause recurrent ANE.^{57,58} Mutations in sodium voltage-gated channel alpha subunit 1 and polymorphisms in the adenosine A2A receptor and carnitine palmitoyl transferase II are involved in various AE syndromes.^{59–61} Because the genetic information of mice, such as the data regarding differences in susceptibilities to febrile seizures between mouse strains,⁶² is easily accessible, our mouse model may contribute to further studies in the field of AE.

In conclusion, the present study showed that P8 mice treated with LPS100 + HT can serve as an animal model of cytokine storm-induced AE, such as ANE and HSES. The simplicity of our mouse model should render it useful for studying the pathogenesis of and for developing potential treatments for AE.

Authors' contributions: HK, KS, FK, TI, and MO conducted the experiments and analyzed the data; MO analyzed the data; YS critically reviewed the results and the manuscript; HK and TM wrote the manuscript; HK, YM, and TM designed and supervised the study.

ACKNOWLEDGMENTS

We thank Dr E. Ohama for his advice on the histopathological findings. This research was partly performed at the Tottori Bio Frontier managed by the Tottori prefecture.

DECLARATION OF CONFLICTING INTERESTS

The authors declared no potential conflicts of interest with respect to the research, authorship, and/or publication of this article.

FUNDING

This work was supported by the JSPS KAKENHI Grant-in-Aid for Scientific Research (C) (17K16264) and the Grants-in-Aid for Tottori University School of Medicine Research.

ORCID iD

Hirofumi Kurata  <https://orcid.org/0000-0001-7203-2405>

REFERENCES

- Hoshino A, Saitoh M, Oka A, Okumura A, Kubota M, Saito Y, Takanashi J, Hirose S, Yamagata T, Yamanouchi H, Mizuguchi M. Epidemiology of acute encephalopathy in Japan, with emphasis on the association of viruses and syndromes. *Brain Dev* 2012;**34**:337–43
- Mizuguchi M, Yamanouchi H, Ichihama T, Shiomi M. Acute encephalopathy associated with influenza and other viral infections. *Acta Neurol Scand Suppl* 2007;**186**:45–56
- Aiba H, Mochizuki M, Kimura M, Hojo H. Predictive value of serum interleukin-6 level in influenza virus-associated encephalopathy. *Neurology* 2001;**57**:295–9
- Morishima T, Togashi T, Yokota S, Okuno Y, Miyazaki C, Tashiro M, Okabe N. Collaborative Study Group on Influenza-Associated Encephalopathy in Japan. Encephalitis and encephalopathy associated with an influenza epidemic in Japan. *Clin Infect Dis* 2002;**35**:512–7
- Ichihama T, Endo S, Kaneko M, Isumi H, Matsubara T, Furukawa S. Serum cytokine concentrations of influenza-associated acute necrotizing encephalopathy. *Pediatr Int* 2003;**45**:734–6
- Mizuguchi M, Abe J, Mikkaichi K, Noma S, Yoshida K, Yamanaka T, Kamoshita S. Acute necrotizing encephalopathy of childhood: a new syndrome presenting with multifocal, symmetric brain lesions. *J Neurol Neurosurg Psychiatry* 1995;**58**:555–61
- Levin M, Hjelm M, Kay JD, Pincott JR, Gould JD, Dinwiddie R, Matthew DJ. Haemorrhagic shock and encephalopathy: a new syndrome with a high mortality in young children. *Lancet* 1983;**2**:64–7
- Mizuguchi M, Hayashi M, Nakano I, Kuwashima M, Yoshida K, Nakai Y, Itoh M, Takashima S. Concentric structure of thalamic lesions in acute necrotizing encephalopathy. *Neuroradiology* 2002;**44**:489–93
- Nakai Y, Itoh M, Mizuguchi M, Ozawa H, Okazaki E, Kobayashi Y, Takahashi M, Ohtani K, Ogawa A, Narita M, Togashi T, Takashima S. Apoptosis and microglial activation in influenza encephalopathy. *Acta Neuropathol* 2003;**105**:233–9
- Kuki I, Shiomi M, Okazaki S, Kawawaki H, Tomiwa K, Amo K, Togawa M, Ishikawa J, Rinka H. Characteristic neuroradiologic features in hemorrhagic shock and encephalopathy syndrome. *J Child Neurol* 2015;**30**:468–75
- Van Acker KJ, Roodhooft AM, Van Bever H. Haemorrhagic shock and encephalopathy. *Eur J Pediatr* 1986;**145**:66–9
- Schrager GO, Shah A. Haemorrhagic shock/encephalopathy syndrome in infancy. *Lancet* 1983;**2**:396
- Bacon CJ. Heatstroke and haemorrhagic shock and encephalopathy. *Lancet* 1983;**2**:918
- Trounce JQ, Lowe J, Lloyd BW, Johnston DI. Haemorrhagic shock encephalopathy and sudden infant death. *Lancet* 1991;**337**:202–3
- Thébaud B, Husson B, Navelet Y, Huault G, Landrieu P, Devictor D, Sebire G. Haemorrhagic shock and encephalopathy syndrome: neurological course and predictors of outcome. *Intensive Care Med* 1999;**25**:293–9
- Takahashi M, Yamada T, Nakashita Y, Saikusa H, Deguchi M, Kida H, Tashiro M, Toyoda T. Influenza virus-induced encephalopathy: clinicopathologic study of an autopsied case. *Pediatr Int* 2000;**42**:204–14
- Bratton SL, Jardine DS. Cerebral infarction complicating hemorrhagic shock and encephalopathy syndrome. *Pediatrics* 1992;**90**:626
- Wu X, Wu W, Pan W, Wu L, Liu K, Zhang HL. Acute necrotizing encephalopathy: an underrecognized clinicoradiologic disorder. *Mediators Inflamm* 2015;**2015**:792578
- Tanaka T, Sunden Y, Sakoda Y, Kida H, Ochiai K, Umemura T. Lipopolysaccharide treatment and inoculation of influenza A virus results in influenza virus-associated encephalopathy-like changes in neonatal mice. *J Neurovirol* 2010;**16**:125–32
- Schwarz JM, Bilbo SD. LPS elicits a much larger and broader inflammatory response than *Escherichia coli* infection within the hippocampus of neonatal rats. *Neurosci Lett* 2011;**497**:110–5
- Dinel AL, Joffre C, Trifilieff P, Aubert A, Foury A, Le Ruyet P, Layé S. Inflammation early in life is a vulnerability factor for emotional behavior at adolescence and for lipopolysaccharide-induced spatial memory and neurogenesis alteration at adulthood. *J Neuroinflammation* 2014;**11**:155
- Eun BL, Abraham J, Mlsna L, Kim MJ, Koh S. Lipopolysaccharide potentiates hyperthermia-induced seizures. *Brain Behav* 2015;**5**:e00348
- Stolp HB, Dziegielewska KM, Ek CJ, Habgood MD, Lane MA, Potter AM, Saunders NR. Breakdown of the blood-brain barrier to proteins in white matter of the developing brain following systemic inflammation. *Cell Tissue Res* 2005;**320**:369–78
- Wu CH, Wang HJ, Wen CY, Lien KC, Ling EA. Response of amoeboid and ramified microglial cells to lipopolysaccharide injections in postnatal rats – a lectin and ultrastructural study. *Neurosci Res* 1997;**27**:133–41
- Stolp HB, Dziegielewska KM, Ek CJ, Potter AM, Saunders NR. Long-term changes in blood-brain barrier permeability and white matter following prolonged systemic inflammation in early development in the rat. *Eur J Neurosci* 2005;**22**:2805–16
- Wang P, You SW, Yang YJ, Wei XY, Wang YZ, Wang X, Hao DJ, Kuang F, Shang LX. Systemic injection of low-dose lipopolysaccharide fails to break down the blood-brain barrier or activate the TLR4-MyD88 pathway in neonatal rat brain. *Int J Mol Sci* 2014;**15**:10101–15
- Yang L, Sameshima H, Ikeda T, Ikenoue T. Lipopolysaccharide administration enhances hypoxic-ischemic brain damage in newborn rats. *J Obstet Gynaecol Res* 2004;**30**:142–7
- Baram TZ, Gerth A, Schultz L. Febrile seizures: an appropriate-aged model suitable for long-term studies. *Brain Res Dev Brain Res* 1997;**98**:265–70
- Patterson KP, Brennan GP, Curran M, Kinney-Lang E, Dubé C, Rashid F, Ly C, Obenaus A, Baram TZ. Rapid, coordinate inflammatory responses after experimental febrile status epilepticus: implications for epileptogenesis. *eNeuro* 2015;**2**:1–12
- Feng B, Tang Y, Chen B, Xu C, Wang Y, Dai Y, Wu D, Zhu J, Wang S, Zhou Y, Shi L, Hu W, Zhang X, Chen Z. Transient increase of interleukin-1 β after prolonged febrile seizures promotes adult epileptogenesis through long-lasting upregulating endocannabinoid signaling. *Sci Rep* 2016;**6**:1–11
- Dubé CM, Ravizza T, Hamamura M, Zha Q, Keebaugh A, Fok K, Andres AL, Nalcioğlu O, Obenaus A, Vezzani A, Baram TZ. Epileptogenesis provoked by prolonged experimental febrile seizures: mechanisms and biomarkers. *J Neurosci* 2010;**30**:7484–94
- Toth Z, Yan XX, Haftoglou S, Ribak CE, Baram TZ. Seizure-induced neuronal injury: vulnerability to febrile seizures in an immature rat model. *J Neurosci* 1998;**18**:428594
- Auvin S, Porta N, Nehlig A, Lécointe C, Vallée L, Bordet R. Inflammation in rat pups subjected to short hyperthermic seizures enhances brain long-term excitability. *Epilepsy Res* 2009;**86**:12430
- Miyata S, Morita S. A new method for visualization of endothelial cells and extravascular leakage in adult mouse brain using fluorescein isothiocyanate. *J Neurosci Methods* 2011;**202**:9–16
- Shen Q, Wang Y, Kokovay E, Lin G, Chuang SM, Goderie SK, Roysam B, Temple S. Adult SVZ stem cells lie in a vascular niche: a quantitative analysis of niche cell-cell interactions. *Cell Stem Cell* 2008;**3**:289–300
- Tavazoie M, Van der Veken L, Silva-Vargas V, Louissaint M, Colonna L, Zaidi B, Garcia-Verdugo JM, Doetsch F. A specialized vascular niche for adult neural stem cells. *Cell Stem Cell* 2008;**3**:27988
- Bennett L, Yang M, Enikolopov G, Iacovitti L. Circumventricular organs: a novel site of neural stem cells in the adult brain. *Mol Cell Neurosci* 2009;**41**:337–47
- Hulse RE, Winterfield J, Kunkler PE, Kraig RP. Astrocytic clasmotodendrosis in hippocampal organ culture. *Glia* 2001;**33**:169–79
- Saunders NR, Dziegielewska KM, Møllgård K, Habgood MD. Markers for blood-brain barrier integrity: how appropriate is Evans blue in the twenty-first century and what are the alternatives? *Front Neurosci* 2015;**9**:385
- Yen LF, Wei VC, Kuo EY, Lai TW. Distinct patterns of cerebral extravasation by Evans Blue and sodium fluorescein in rats. *PLoS One* 2013;**8**:e68595
- Wolman M, Klatzo I, Chui E, Wilmes F, Nishimoto K, Fujiwara K, Spatz M. Evaluation of the dye-protein tracers in pathophysiology of the blood-brain barrier. *Acta Neuropathol* 1981;**54**:55–61

42. Liu WY, Wang ZB, Wang Y, Tong LC, Li Y, Wei X, Luan P, Li L. Increasing the permeability of the blood – brain barrier in three different models in vivo. *CNS Neurosci Ther* 2015;**21**:568–74
43. Hickey E, Shi H, Van Arsdell G, Askalan R. Lipopolysaccharide-induced preconditioning against ischemic injury is associated with changes in Toll-like receptor 4 expression in the rat developing brain. *Pediatr Res* 2011;**70**:104
44. Banks WA, Gray AM, Erickson MA, Salameh TS, Damodarasamy M, Sheibani N, Meabon JS, Wing EE, Morofuji Y, Cook DG, Reed MJ. Lipopolysaccharide-induced blood-brain barrier disruption: roles of cyclooxygenase, oxidative stress, neuroinflammation, and elements of the neurovascular unit. *J Neuroinflammation* 2015;**12**:223
45. Eklind S, Mallard C, Leverin AL, Gilland E, Blomgren K, Mattsby-Baltzer I, Hagberg H. Bacterial endotoxin sensitizes the immature brain to hypoxic-ischaemic injury. *Eur J Neurosci* 2001;**13**:1101–6
46. Huang H, Fletcher A, Niu Y, Wang TT, Yu L. Characterization of lipopolysaccharide-stimulated cytokine expression in macrophages and monocytes. *Inamm Res* 2012;**61**:1329–38
47. Tomimoto H, Akiguchi I, Wakita H, Suenaga T, Nakamura S, Kimura J. Regressive changes of astroglia in white matter lesions in cerebrovascular disease and Alzheimer's disease patients. *Acta Neuropathol* 1997;**94**:146–52
48. Sahlas DJ, Bilbao JM, Swartz RH, Black SE. Clasmotodendrosis correlating with periventricular hyperintensity in mixed dementia. *Ann Neurol* 2002;**52**:378–81
49. Arai N. The role of swollen astrocytes in human brain lesions after edema – an immunohistochemical study using formalin-fixed paraffin-embedded sections. *Neurosci Lett* 1992;**138**:56–8
50. Misu T, Höftberger R, Fujihara K, Wimmer I, Takai Y, Nishiyama S, Nakashima I, Konno H, Bradl M, Garzuly F, Itoyama Y, Aoki M, Lassmann H. Presence of six different lesion types suggests diverse mechanisms of tissue injury in neuromyelitis optica. *Acta Neuropathol* 2013;**125**:815–27
51. Shimoda K, Mimaki M, Fujino S, Takeuchi M, Hino R, Uozaki H, Hayashi M, Oka A, Mizuguchi M. Brain edema with clasmotodendrosis complicating ataxia telangiectasia. *Brain Dev* 2017;**39**:629–32
52. Tachibana M, Mohri I, Hirata I, Kuwada A, Kimura-Ohba S, Kagitani-Shimono K, Fushimi H, Inoue T, Shiomi M, Kakuta Y, Takeuchi M, Murayama S, Nakayama M, Ozono K, Taniike M. Clasmotodendrosis is associated with dendritic spines and does not represent autophagic astrocyte death in influenza-associated encephalopathy. *Brain Dev* 2019;**41**:85–95
53. Hase Y, Craggs L, Hase M, Stevenson W, Slade J, Lopez D, Mehta R, Chen A, Liang D, Oakley A, Ihara M, Horsburgh K, Kalaria RN. Effects of environmental enrichment on white matter glial responses in a mouse model of chronic cerebral hypoperfusion. *J Neuroinflammation* 2017;**14**:81
54. Kim JE, Ryu HJ, Yeo SI, Seo CH, Lee BC, Choi IG, Kim DS, Kang TC. Differential expressions of aquaporin subtypes in astroglia in the hippocampus of chronic epileptic rats. *Neuroscience* 2009;**163**:781–9
55. Yoshimura H, Imai Y, Beppu M, Ohara N, Kobayashi J, Kuzuya A, Yamagami H, Kawamoto M, Kohara N. Elderly autopsy case of influenza-associated encephalopathy. *Rinsho Shinkeigaku* 2008;**48**:713–20
56. Yamada S, Yasui K, Hasegawa Y, Tsuzuki T, Yoshida M, Hashidume Y. An autopsy case of pandemic (H1N1) 2009 influenza virus-associated encephalopathy. *Rinsho Shinkeigaku* 2012;**52**:480–5
57. Fukasawa T, Kubota T, Negoro T, Saitoh M, Mizuguchi M, Ihara Y, Ishii A, Hirose S. A case of recurrent encephalopathy with SCN2A missense mutation. *Brain Dev* 2015;**37**:631–4
58. Neilson DE, Adams MD, Orr CM, Schelling DK, Eiben RM, Kerr DS, Anderson J, Bassuk AG, Bye AM, Childs AM, Clarke A, Crow YJ, Di Rocco M, Dohna-Schwake C, Dueckers G, Fasano AE, Gika AD, Giannis D, Gorman MP, Grattan-Smith PJ, Hackenberg A, Kuster A, Lentschig MG, Lopez-Laso E, Marco EJ, Mastroianni S, Perrier J, Schmitt-Mechelke T, Servidei S, Skardoutsou A, Uldall P, van der Knaap MS, Goglin KC, Tefft DL, Aubin C, de Jager P, Hafler D, Warman ML. Infection-Triggered familial or recurrent cases of acute necrotizing encephalopathy caused by mutations in a component of the nuclear pore, RANBP2. *Am J Hum Genet* 2009;**84**:44–51
59. Saitoh M, Shinohara M, Hoshino H, Kubota M, Amemiya K, Takanashi JL, Hwang SK, Hirose S, Mizuguchi M. Mutations of the SCN1A gene in acute encephalopathy. *Epilepsia* 2012;**53**:558–64
60. Shinohara M, Saitoh M, Nishizawa D, Ikeda K, Hirose S, Takanashi J, Takita J, Kikuchi K, Kubota M, Yamanaka G, Shiihara T, Kumakura A, Kikuchi M, Toyoshima M, Goto T, Yamanouchi H, Mizuguchi M. ADORA2A polymorphism predisposes children to encephalopathy with febrile status epilepticus. *Neurology* 2013;**80**:1571–6
61. Shinohara M, Saitoh M, Takanashi J, Yamanouchi H, Kubota M, Goto T, Kikuchi M, Shiihara T, Yamanaka G, Mizuguchi M. Carnitine palmitoyl transferase II polymorphism is associated with multiple syndromes of acute encephalopathy with various infectious diseases. *Brain Dev* 2011;**33**:512–7
62. Van Gassen KL, Hessel EV, Ramakers GM, Notenboom RG, Wolterink-Donselaar IG, Brakkee JH, Godschalk TC, Qiao X, Spruijt BM, van Nieuwenhuizen O, de Graan PN. Characterization of febrile seizures and febrile seizure susceptibility in mouse inbred strains. *Genes, Brain Behav* 2008;**7**:578–86

(Received February 10, 2019, Accepted April 1, 2019)